All optical switches based on the coupling of surface plasmon polaritons

G. Margheri, T. Del Rosso, S.Sottini, S. Trigari, and E.Giorgetti

Istituto dei Sistemi Complessi, Consiglio Nazionale delle Ricerche, via Madonna del Piano 10, Sesto Fiorentino (Firenze), 50019, Italy
Corresponding author: giancarlo.margheri@isc.cnr.it

Abstract: We studied the potentials of All Optical Switches (AOS) based on the intensity-dependent coupling and decoupling of light into the SPP modes (Surface Plasmon Polaritons) of a sinusoidally corrugated thin metal film (TMF), due to Kerr induced refractive index changes of the surrounding dielectrics. The ideal device has two spatially separated outputs, collecting the reflected and transmitted light and the active volume can be as small as 10^{-2} mm^3. Gold and PTS (poly-(2,4-hexadiyne-1,6-diol bis(p-toluene sulfonate) are the materials considered. Losses are limited to 1.5 dB,while a 20 dB extinction ratio per gate has been theoretically demonstrated with signal pulsewidths of 5-10 ps , using a maximum optical switching peak power of 11 kW.

OCIS codes: (230.1150) All-optical devices; (240.6680) Surface plasmons ; (160.4330) Nonlinear optical material

References and links

1. S. I. Bozhevolnyi,V. S.Volkov,E. Devaux,and T. W. Ebbesen, "Channel plasmon polaritons guided by subwavelength metal grooves," Phys. Rev. Lett. **95**, 046802-046804 (2005).
2. V. A. Markel, and A. K. Sarychev, "Propagation of surface plasmons in ordered and disordered chains of metal nanospheres," Phys. Rev. B **75**, 085426-085437 (2007).
3. W. Saj, "FDTD simulations of 2D plasmon waveguide on silver nanorods in hexagonal lattice," Opt. Express **13**, 4818-4827 (2005).
4. Y. Jiang, Z. Cao, G. Chen, X. Dou, and Y.Chen, "Low voltage electro-optic polymer light modulator using attenuated total internal reflection," Opt. Laser Technol. **33**, 417-420 (2001).
5. A. Giannattasio,I. R. Hooper,and W. L. Sambles, " Transmission of light through thin silver films via surface plasmon polaritons," Opt. Express, **12**, 5881-5886 (2004).
6. I. R. Hooper and J. R. Sambles, "Coupled surface plasmon polaritons on thin metal slabs corrugated on both surfaces," Phys. Rev. B **70**, 045421-045435 (2004).
7. W. L. Barnes,T. W. Preist,S. C. Kitson, and J. R. Sambles "Physical origin of photonic energy gaps in the propagation of surface plasmons on gratings," Phys. Rev. B, **54**, 6227-6244 (1996).
8. R. Dragila. B. Luther-Davies, and S.Vukovic, "High Transparency of Classically Opaque Metallic Films," Phys. Rev. Lett. **55**, 1117-1120 (1985).
9. E. Giorgetti, G. Margheri, T. DelRosso, and S. Sottini, "Periodic Metal-Dielectric Interfaces for Photonic Applications," Laser Physics **18**, 1-6 (2008).
10. J. Wang, J. Sun, and Q. Sun, "Experimental observation of a 1.5 μm band wavelength conversion and logic NOT gate at 40 Gbit/s based on sum-frequency generation," Opt. Lett. **31**, 1711-1713 (2006).
11. J. Wang, J. Sun, and Q. Sun, "Single-PPLN-based simultaneous half-adder, half-subtracter, and OR logic gate: proposal and simulation," Opt. Express **15**, 1690-1699 (2007).
12. M. Kahl, and E. Voges, "Analysis of plasmon resonance and surface enhanced Raman scattering on periodic silver structures," Phys. Rev. B **61**, 14078-14088 (2000).
13. J. Chandezon, M. T. Dupuis, and G. Cornet, "Multicoated gratings: a differential formalism applicable in the entire optical region," J. Opt. Soc. Am. **72**, 839-846 (1982).
14. A. Feldner, W. Reichstein, T. Vogtmann, M. Schwoerer, L. Friedrich, T. Pliska, M. Liu, G. Stegeman, and Seung-Han Park, "Linear optical properties of polydiacetylene para-toluene sulfonate thin films," Opt. Commun. **195**, 205-209 (2001).
15. R. J. Crook, J. R. Sambles, R. Rangel-Sojo, G. Spruce, and B. S. Wherrett, "The electronic nonlinear optical behaviour of a grating coupled polymer 9BCMU waveguide," J. Phys. D **28**, 269–274 (1995).
16. L. G. Schulz, "The optical constants of silver, gold, copper and aluminum. I. the absorption coefficient k," J. Opt. Soc. Am. **44**, 357-362 (1954).

#93140 - $15.00 USD Received 25 Feb 2008; revised 3 Apr 2008; accepted 3 Apr 2008; published 20 Jun 2008

17. L. G. Schulz, and F. R. Tangherlini, "Optical constants of silver, gold, copper, and aluminum. II. The index of refraction n," J. Opt. Soc. Am. **44**, 362-368 (1954).
18. S. Polyakov, F. Yoshino, M. Liu, and G. Stegeman, "Nonlinear refraction and multiphoton absorption in polydiacetylenes from 1200 to 2200 nm," Phys. Rev. B. **69**, 115421 (2004).
19. A. Melloni, M. Chinello, and M. Martinelli, "All-optical switching in phase-shifted fiber Bragg grating," IEEE Photonics Technol. Lett. **12**, 42-44 (2000).
20. S. La Rochelle, Y. Hibino, V. Mizrahi, and G. I. Stegeman, "All-optical switching of grating transmission using cross-phase modulation in optical fibers," Electron Lett. **26**, 1459-1460 (1990).
21. G. Margheri,A. Mannoni, and F.Quercioli, "High resolution angular and displacement sensing based on the excitation of surface plasma waves," Appl. Opt. **36**, 4521-4525 (1997).
22. E. D. Palik, *Handbook of Optical Constant of Solid III*, (Academic Press,1998).
23. S. H. Zaidi, D. W. Reicher, B. Draper, J. R. McNeil, and S. R. J. Brueck, "Characterization of Thin Al Films using Grating Coupling to Surface Plasma Waves," J. Appl. Phys. **71**, 6039-6048 (1992).
24. M. J. Poulter, D. Neely, J. Collier, and C. Danson, " Transmission grating CPA system design for the Vulcan laser," Central Laser Facility Annual Report, 2000/2001, 157-159.
25. G. Margheri, E. Giorgetti, S. Sottini, and G. Toci, "Nonlinear characterization of nanometer-thick dielectric layers by surface plasmon resonance techniques," J.Opt.Soc.Am **20**, 741-751 (2003).
26. V. M. Shalaev, and A. K. Sarychev, "Nonlinear optics of random metal-dielectric films," Phys. Rev. B **57**, 13265-13288 (1998).
27. R. J. Gehr, G. L. Fischer, R. W. Boyd, and J. E. Sipe, "Nonlinear optical response of layered composite materials," Phys. Rev. A, **53**, 2792-2798 (1996).
28. F. Hao, C. L. Nehl, J. H. Hafner, and P. Nordlander, "Plasmon resonances of a gold nanostar," Nano Lett. **7**, 729-732 (2007).
29. S. L. Westcott, S. J. Oldenburg, T. R. Lee, and N. J. Halas, "Construction of simple gold nanoparticle aggregates with controlled plasmon–plasmon interactions," Chem. Phys. Lett. **300**, 651-655 (1999).

1. Introduction

Communications and processing systems must deal with huge amounts of data at ever increasing velocity. Electronic and optical circuits are currently investigated to overcome the present technological limits. Due to the different nature of electrons and photons, electronic and optical devices usually show complementary characteristics in terms of sizes, speed, etc. At present, while the research activity in electronics pursues the objective to push a consolidated technology to the limit, many progress steps must be reached before conceiving competitive photonic signal processors. For this goal, however, the typical dimensions of conventional dielectric optical waveguides, which are dictated by diffraction limit, prevent dense on-chip integration with electronic devices.

Recently, the possibility of combining nanotechnology and photonics opened new interesting scenarios to overcome the size problems. In addition to photonic crystal structures and, in case, combined with them, plasmonics seems to be particularly promising to achieve both the compactness of electronics and the speed of optics. In particular, there is a growing research interest in plasmonic structures, such as channel plasmons waveguides [1] **,** chains of nanoparticles [2], nanorods [3] etc, which guide light through the interaction of photons and electron oscillations at a metal surface and permit development of nanoscale optical elements. However the trade-off between confinement level and propagation losses is a fundamental limit of such waveguides.

The previous considerations stimulated the investigation of photonic devices such as electro-optic (EO) modulators based on reflection geometry [4]. Many of these studies involve the modulation of the Attenuated Total internal Reflection (ATR) of light, which is associated with the excitation of Surface Plasmon Polaritons (SPPs). In this case, since this geometry does not require long range SPP propagation, the losses are no more a major concern as it happens in usual integrated optics. Nevertheless a reduction of SPP propagation losses induces a narrowing of the resonance conditions required for SPP coupling with consequent improvement of the sensitivity of the device [4]. SPPs coupled to corrugated Thin Metal Films (TMF) have also been studied as alternatives to more complicated 2D nanostructures, in order to exploit their capability of enhancing the transmission of light from the incidence to the substrate medium [5]. Both conformal and nonconformal periodically modulated TMF were examined in the ideal case when air is the external medium [6]. In

#93140 - $15.00 USD Received 25 Feb 2008; revised 3 Apr 2008; accepted 3 Apr 2008; published 20 Jun 2008

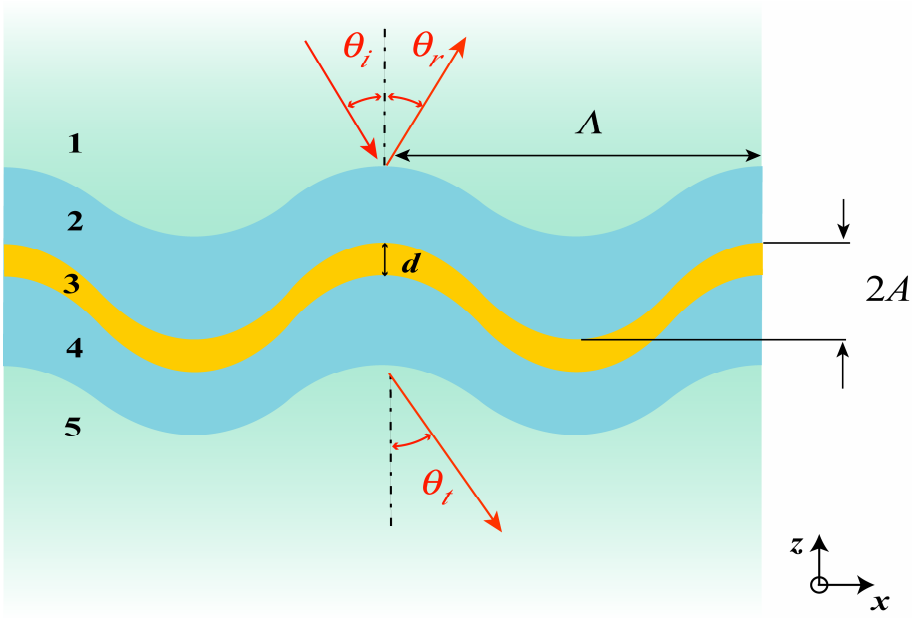

Fig. 1. The stratification considered in the present work.

general, when the TMF is thin enough and the outer media at both sides of the TMF have the same dielectric constants, the structure can support Long Range and Short Range Surface Plasmon Polaritons (LRSPP and SRSPP), which are characterized by different surface charge density distribution and thus by different energies [7]. Their coupling with free propagating radiation via the grating modulation can lead to interesting features both in reflection and in transmission. So in the nonconformal case strongly enhanced transmission through the TMF was observed, which can be almost independent of the angle of incidence [6]. This behaviour may occur also in the case of conformal films, provided that identical dielectrics bound the TMF [6, 8]. Lastly conformal gratings generating photonic band-gaps for SPPs have also been reported [6, 9].

In this work the potentials of All Optical Switches (AOS) based on the SPP modes of a sinusoidally corrugated TMF are considered, by supposing that the corrugated TMF is bounded by identical dielectrics with third order optical nonlinearity (NL). The investigated devices exploit the intensity-dependent coupling and decoupling of light into the SPP modes, as the SPP wavevector is shifted by Kerr induced refractive index changes. The ideal device has two spatially separated outputs collecting the reflected and transmitted light. Each channel has an ON and an OFF state, complementary to that of the other channel and triggered by the ON-OFF status of the nonlinearity. Paragraph 2 describes the theoretical modelling of light coupling to sinusoidally corrugated gold TMF. The reflected and transmitted beams are calculated as a function of the device parameters and, in particular, of the NL characteristics of the dielectrics bounding the TMF. Paragraph 3 is devoted to a critical survey of presently available technologies and NL materials which could be adopted, now or in a near future, to develop our AOS. To finish with, we emphasize that the optical switching can be easily extended to logic gates. For example, various logic gates such as NOT, AND, XOR could be performed based on the similar operation principles to optical switching [10,11].

2. Modelling

We modelled SPP-based AOSs by referring to the structure sketched in Fig. 1. It consists of

#93140 - $15.00 USD Received 25 Feb 2008; revised 3 Apr 2008; accepted 3 Apr 2008; published 20 Jun 2008

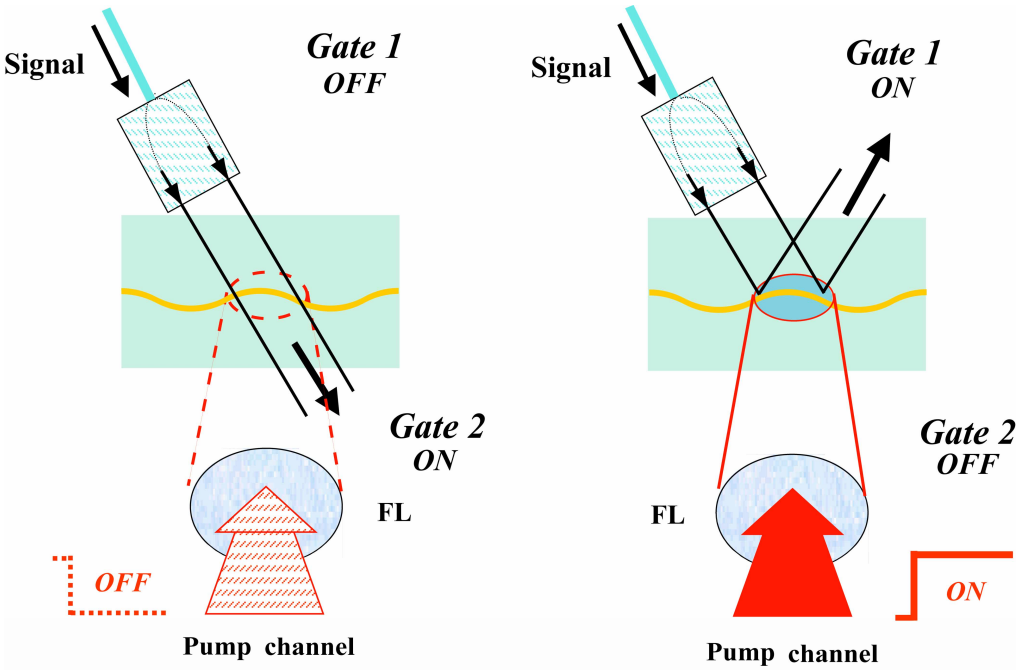

Fig. 2. Working scheme of an AOS based on refractive index change: signal from a fiber ended by a GRIN (graded index) rod is transmitted or reflected by the nonlinear structure according to whether the pump, coming transversally through a focusing lens FL, is ON or OFF.

five media, which are characterized by dielectric constants ε_i (i = 1, 2…5); **1**, **2**, **4** and **5** are dielectrics (**1** and **5** can be air) and **3** is a coinage metal film. The media are separated by sinusoidally corrugated interfaces, where A is the amplitude and Λ the period of the modulation. Let us suppose that $Re(\varepsilon_3)$ is < 0 and $Re(\varepsilon_{2,4})$ are > 0. If media **2**, **4** are very thick and also the thickness of the TMF can be considered large (> 20 nm at VIS-NIR wavelengths), then independent coupling of SPPs is possible at **2** - **3** or **4** - **3** interfaces with wavevectors $k_{SPP\,2,4}$. We limited our investigation to the case when the metal film is thin (10 - 20 nm thickness) and media **2** and **4** are identical. In this case a single interface SPP can no longer exist and two modes can be excited with the same wavevector (LRSPP and SRSPP). These modes exhibit a more complex dispersion relationship with respect to that of the single interface SPP. In the case of semi infinite media **2** and **4** it is given by the following equation:

$$\tanh\left(p_3\, d\right) = -\frac{\Gamma_3\left(\Gamma_4 + \Gamma_2\right)}{\Gamma_3^{\,2} + \Gamma_4\Gamma_2}$$

$$\Gamma_i = \frac{p_i}{\varepsilon_i} \qquad i = 1 \ldots\ldots 5 \qquad (1)$$

$$p_i = \sqrt{k_{SPP\,i}^{\,2} - \varepsilon_i k_0^{\,2}}$$

where d represents the thickness of the metal layer and k_0 the wavevector of light in vacuum. In principle eq. 1 is strictly valid only in the case of a plane TMF, however it is a good approximation also in the case of small corrugations like those considered in this work [12]. It has two independent solutions. The high frequency one, LRSPP, has low inner damp because field inside the metal has a lower amplitude than for the SRSPP. Consequently its propagation can occur even for millimeter ranges, so assuring a high sensitivity of the structure to

#93140 - $15.00 USD Received 25 Feb 2008; revised 3 Apr 2008; accepted 3 Apr 2008; published 20 Jun 2008

refractive index changes. In practice light can be coupled to LRSPPs according to the following condition:

$$k\sin(\theta_i) \pm m\,K = \pm k_{\mathrm{LRSPP}} \qquad m = 1..... n \qquad (2)$$

where k is the magnitude of the wave vector of the incident light, θ_t is the incidence angle, k_{LRSPP} is the magnitude of the wave vector associated with the LRSPP mode, $K = 2\,\pi/\Lambda$ is the magnitude of the Bragg vector of the grating and the integer m is the order of the scattering process.

Once excited (for symmetry reasons there is no difference if the incidence medium is **2** or **4** of Fig. 1), the SPP can be scattered by the grating and thus converted back into light. Due to phase mismatch, the intensity of the reflected beam at angle θ_r drops down. But the SPP excited at interface **2** - **3** couples with the SPP of interface **3** - **4**, that in turn can again convert via the grating interaction to transmitted light at angle θ_t in medium **4** [5]**.** The scattering capabilities of this LRSPP-supporting device can be exploited to obtain an AOS with two output gates. The working principle relies on the spectral response shift induced by the Kerr change of the refractive index of one or both layers **2**, **4** in contact with the TMF. Fig. 2 reports a sketch of a possible device. Four pigtails (short lengths of fibre permanently attached to the device) are necessary: one for the input signal, two for the outputs of the switch (Gate 1 and 2) and the fourth for the switching pump beam [6]. The signal beam, constituted by a train of temporal Gaussian-like pulses, in general, cannot be used directly as the pump: a distinct channel is required whose polarization must be normal to the TMF, since all the SPP are TM modes.

For the modelling of the AOS, we chose the dielectric constants and the thicknesses of the different media so that only one LRSPP could be coupled, corresponding to $m = 1$ in eq. 2. The interface profiles are conformal and described by the following relation:

$$f(x) = A\sin(Kx) \qquad (3)$$

The computer code for the AOS modelling is based upon the method originally proposed by Chandezon, *et al*., ii [13], who first constructed a differential formalism to find the reflected and the transmitted intensity of a multicoated grating fed by a plane, monochromatic wave. In the modelling of our AOS, we considered the following main tasks:

1 The extinction ratio $\eta = S_{max}/S_{min}$ between the output signals in the ON and OFF state of

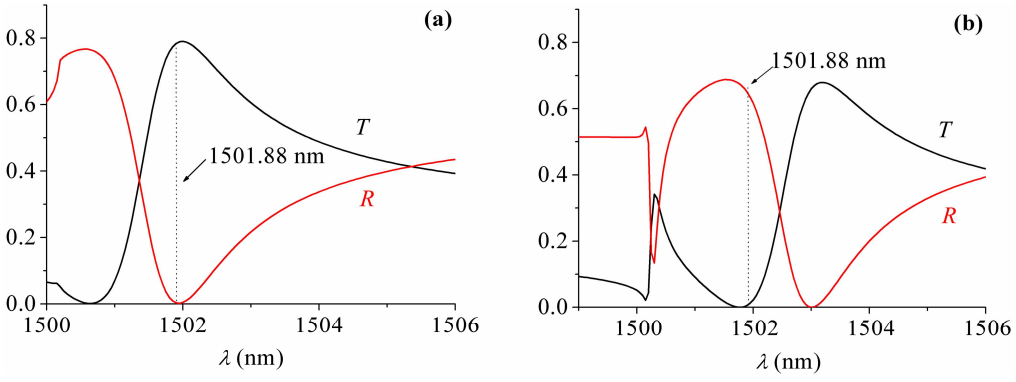

Fig. 3. Reflectivity *R* and transmittivity *T* of the AOS with 1 NL layer (4): (a) OFF state, (b) ON state.

#93140 - $15.00 USD Received 25 Feb 2008; revised 3 Apr 2008; accepted 3 Apr 2008; published 20 Jun 2008

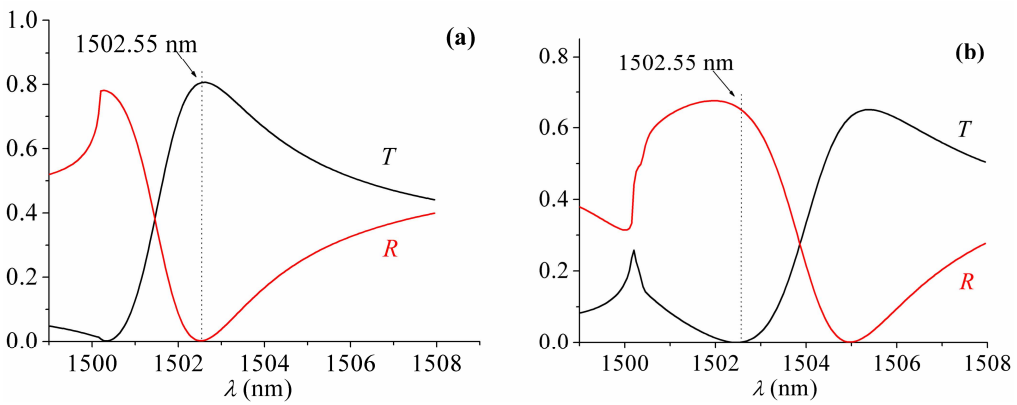

Fig. 4. Reflectivity *R* and transmittivity *T* of the AOS with 2 NL layers (2, 4): (a) OFF state, (b) ON state.

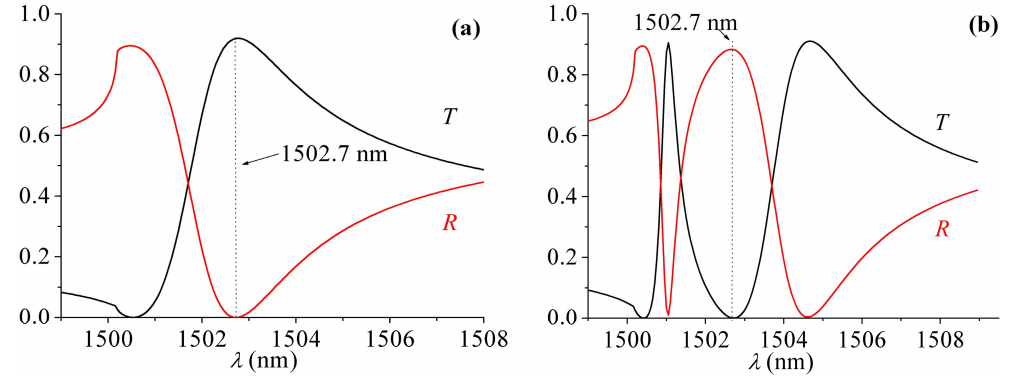

Fig. 5. Reflectivity *R* and transmittivity *T* of the AOS with 1 NL layer (4) with only real NL refractive index,increased of 35 % with respect to the corresponding case with complex nonlinearity: (a) OFF state, (b) ON state.

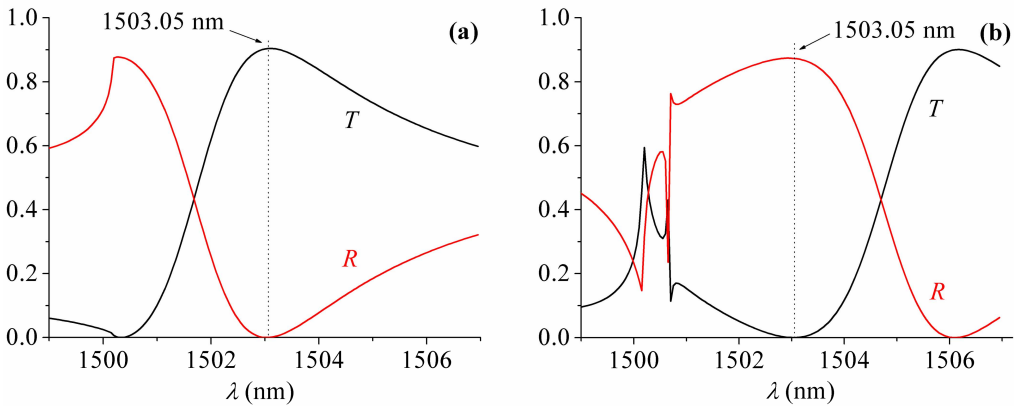

Fig. 6. Reflectivity *R* and transmittivity *T* of the AOS with 2 NL layers (2, 4) with only real NL refractive index,increased of 25 % with respect to the corresponding case with complex nonlinearity: (a) OFF state, (b) ON state.

#93140 - $15.00 USD Received 25 Feb 2008; revised 3 Apr 2008; accepted 3 Apr 2008; published 20 Jun 2008

the switch at the same gate must be as high as possible, in order to enhance the signal to noise ratio (S/N). A figure of $\cong$ 20 dB was our target, with S_{max} (normalized to 1) of the order of 0.70.

2 A switching peak intensity of the pump $\cong$ 5 GW/cm^2, or smaller, provide that it can be fed by optical fibre amplifiers. Moreover, as it will be discussed later on, this intensity level can be managed with low risks of material damaging [14, 15].

3 The dimensions of the active device must be sub-mm.

4 Another challenging requirement of our modelling activity was that of balancing the NL effects in reflection and in transmission (namely the two output channels), at the same wavelength and for the ON-OFF states.

The home-made computer code for the AOS modelling is based upon the method originally proposed by Chandezon et alii [13], who first constructed a differential formalism to find the reflected and the transmitted intensity of a multicoated grating fed by a plane, monochromatic wave. The results of such simulations are reported in § *2.1*. Then in § *2.2*, the AOS model was implemented taking into account the non zero spatial and temporal bandwidths respectively of the input pulses. This will enable us to give the proper dimension of the input beam on the AOS and to derive the value of the active volume (§ *2.3*).

2.1 Monochromatic plane wave input

Let us focus now on some particular cases which can give an idea of the potentials of the AOS structures we have studied. The parameters, which characterize the different configurations, are the grating period and amplitude, the metal film thickness, the dielectric constants, the NL behaviour of layers **2** and **4**, the peak power of the switching beam and the minimum size of the light spot impinging on the AOS. We supposed that, in the OFF state of the nonlinearity, media **2** and **4** have the low-intensity refractive index of 1.75, namely that of polydiacetylene PTS (poly-(2,4-hexadiyne-1,6-diol bis(p-toluene sulfonate))) films at 1500 nm [14] and that medium **3** is gold, with dielectric constant ε_{Au} = - 108 + 5.464 *i* at 1500 nm [16, 17]**.** Media **1** and **5** are linear and with the same dielectric constant as media **2** and **4**. The θ_t angle of the impinging wave was 8°. The reason for this choice will be discussed extensively later.

We considered first the case when only layer **4** is NL and exhibits the properties of PTS at 1500 nm (n_2 = 7 x10^{-4} cm^2/ GW, α_3 = 1 cm^3/GW^2) [18]. Assuming a thickness of the metal and of the NL film of 11 nm and 6 μm respectively, we optimized the reflectivity *R* and transmittivity *T*, i.e. the fraction of incident radiation reflected and transmitted by the structure corresponding to the OFF-ON states of NL medium, by varying the period and amplitude of the modulation. The best result is reported in Fig. 3 and corresponds to a grating period of 752.5 nm and an amplitude of 30 nm. The previous value of the grating period will be maintained for all the cases considered in this work. As a consequence, the working wavelengths can change slightly in different examples. The switching conditions corresponding to the vertical dotted line of Fig. 3 can be obtained with a variation of the refractive index of the NL medium Δn = 0.0026 + 0.000168 *i*, corresponding to a peak power of 11 kW. By supposing a section of the pump beam equal to 288 μm^2, this value corresponds to an intensity of 3.7 GW/cm^2. The importance and the criteria for the choice of the beam section will be addressed in more detail later.

We then calculated the reflectivity and transmittivity of a structure in which both layers **4** and **2** are NL and, again, exhibit the same NL behaviour as PTS at 1500 nm. They are plotted in Fig. 4 (a), (b). The total thickness of the NL material is now 9 μm (4.5 μm x 2), instead of 6 μm. A slight increase of the grating amplitude, *A* = 38.5 nm, and of the gold thickness *d* = 11.7 nm, was necessary to optimize the AOS performance. Since a section of the pump beam equal to 225 μm^2 is now sufficient, a peak power of 11 kW yields an intensity of 4.8 GW/cm^2, which is able to produce a Δn = 0.0033 + 0.00027 *i*.

For the following two cases we improved the NL parameters, with respect to those

#93140 - $15.00 USD Received 25 Feb 2008; revised 3 Apr 2008; accepted 3 Apr 2008; published 20 Jun 2008

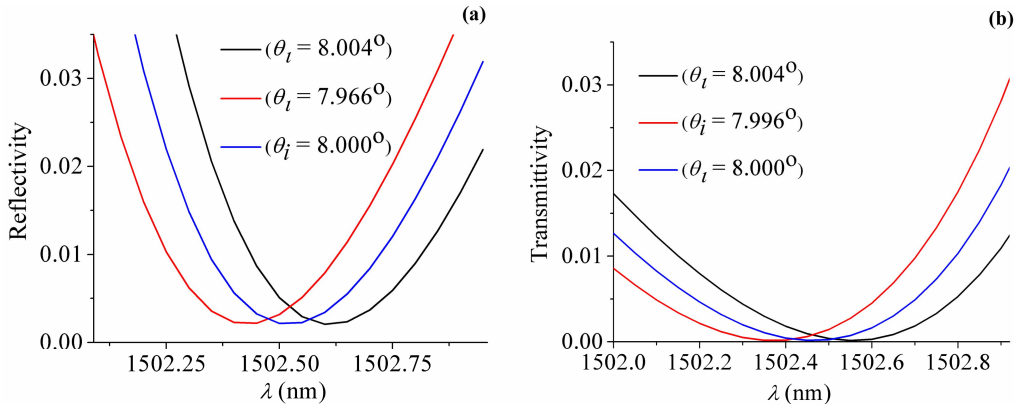

Fig. 7. Reflectivity R (a) and transmittivity T (b) for three incidence angles when the NL is ON and layers 2 and 4 are activated.

exhibited by PTS. First of all, we reduced to zero the imaginary component of Δn. In the case of PTS, this condition can be obtained around 1700 nm [18]. Moreover, the real component was supposed to be 35% and 25% higher than that of PTS in the third and fourth case respectively. Referring to Fig. 5(a), 5(b), the transmittivity and reflectivity are plotted in the OFF and ON states of the AOS, in the case of only one NL layer, layer **4**, whose thickness is again 6 μm. The grating amplitude is 35 nm and the gold thickness is 13 nm. The switching intensity is 4.8 GW/cm^2, corresponding to a purely real $\Delta n = 0.0045$. The last case, which is reported in Fig. 6(a), 6(b), is the analogous of that of Fig. 4(a), 4(b) (both layers **2** and **4** are NL). The grating amplitude was 40 nm, the gold thickness 13 nm. With the same switching intensity of 4.8 GW/cm^2 as in Fig. 4, a $\Delta n = 0.0041$ was achieved. In all examined cases the ON - OFF states of the AOS cause a strong change in the R - T curves. Notice that, when the pump is ON, the presence of a further resonance on the left side is evident. In fact, since the thickness of the illuminated areas can be as large as 9 μm, the significant refractive index increase, with respect to the outer media, permits excitation of the guided TM_1 mode.

Table 1. Response of the AOS to a Gaussian pulse with duration t_0. Extinction ratios η are reported at gate 1 (reflection) and gate 2 (transmission) for two different cases: one nonlinear PTS layer on the bottom of the metal film and two nonlinear PTS layers symmetric sandwiching the film.

	1 Nl layer		**2 Nl layers**	
Δn	0.0026 + 0.000168 i		0.0033 + 0.00027 i	
Angle tolerance	+/- 0.001°		+/- 0.004°	
Pump peak power (kW)	11		11	
Switching intensity (GW/cm^2)	3.7		4.8	
	$\eta = S_{max}/S_{min}$			
Pulse duration t_0 (ps)	**Gate 1**	**Gate 2**	**Gate 1**	**Gate 2**
5	12.6 (0.67*)	12.5 (0.70*)	17.5 (0.78*)	20 (0.81*)
10	16.4	17.2	21.5	23.3
20	20	19.4	24	24.8

* maximum output level

#93140 - $15.00 USD Received 25 Feb 2008; revised 3 Apr 2008; accepted 3 Apr 2008; published 20 Jun 2008

Table 2. Response of the AOS based on an ideal nonlinear material to a Gaussian pulse with duration t_0.

	1 Nl layer		**2 Nl layers**	
Δn	0.0045		0.0041	
Angle tolerance	+/- 0.002°		+/- 0.004°	
Pump peak power (kW)	11		5.5	
Switching intensity (GW/cm^2)	4.8		4.8	
	$\eta = S_{max}/S_{min}$			
Pulse duration t_0 (ps)	**Gate 1**	**Gate 2**	**Gate 1**	**Gate 2**
5	16.8 (0.84*)	17.2 (0.89*)	17.6 (0.87*)	22.6 (0.89*)
10	22.4	22.7	22.3	25.6
20	27.1	27.4	23.8	27.4

* maximum output level

2.2 Input signals with nonzero temporal-spatial bandwidths

In the previous calculations we considered monochromatic plane waves. However, in practical working conditions, the light comes from optical fibres in the form of trains of pulses each one having non negligible bandwidth around the carrier frequency. Moreover, the signal beam is also space-limited because of fiberoptic confinement, so that also a non zero angular spectrum needs to be considered. Therefore, as a further modelling step, we carried out an evaluation of the system performances in the case of non monochromatic beam launched ad different angles, and we will derive the constraints for angular spectrum of the signal input.

The spectra of the typical signal pulses transmitted by optical fibres can be as wide as 0.5 - 1 nm around the carrier frequency. Moreover Gaussian beams show a spatial bandwidth $\Delta\theta$ that depends on the waist radius w_0 and increases as the beam width decreases. This can represent a serious drawback when the signal is processed by a wavelength-selective device, in which the non zero band tails of the signal may experience significant spectral distortions. In particular this effect is expected to have a strong detrimental effect on task #1 of our investigation, that is the 20 dB extinction ratio between the ON-OFF states in each gate of our switch.

We considered a Gaussian time dependence of the electric field E of the input pulse:

$$E(\mathbf{r},t) = E_0\, e^{\,i(\omega t - \mathbf{k}\cdot\mathbf{r})} e^{-\left(\frac{t}{t_0}\right)^2} \tag{4}$$

Its power spectrum is given by:

$$P(\mathbf{r},\omega) = \left|E_\omega(\mathbf{r},\omega)\right|^2 \tag{5}$$

where $E_\omega(\mathbf{r},\omega)$ is the Fourier transform of the input field. By transferring $P(\mathbf{r},\omega)$ in the wavelength domain, thus achieving a new spectral power distribution $P_\lambda(\mathbf{r},\lambda)$, we can write

#93140 - $15.00 USD Received 25 Feb 2008; revised 3 Apr 2008; accepted 3 Apr 2008; published 20 Jun 2008

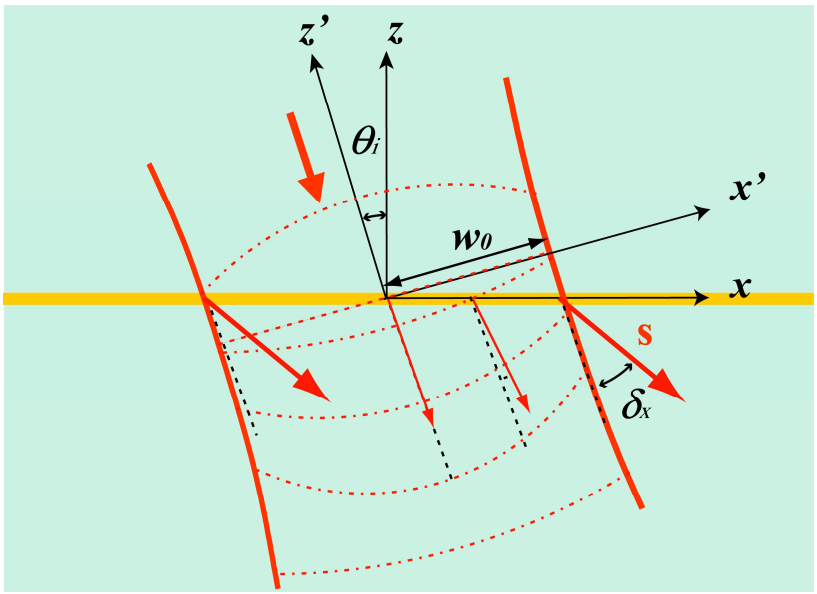

Fig. 8. Signal beam with Gaussian profile TEM_{00} and waist radius w_0 , impinging on the metal film at angle θ_i,. Due to the change of wavefront profile along z', wavevector **s** is tilted by δ_x with respect to the beam direction., so affecting the performance of AOS device.

the correct reflection response of the device as:

$$R(\theta) = \frac{P_R(\theta)}{P_{inc}} \tag{6}$$

with:

$$P_R(\theta) = -\int_0^\infty \frac{P_\lambda(\lambda)\ \mathrm{c}\ R(\lambda,\theta)}{\lambda^2}\, d\lambda \tag{7}$$

$$P_{inc} = -\int_0^\infty \frac{P_\lambda(\lambda)\ \mathrm{c}}{\lambda^2}\, d\lambda \tag{8}$$

where c is the speed of light in vacuum, λ is the wavelength in vacuum, $R(\lambda,\theta_t)$ the reflectivity calculated at the incidence angle θ_t . Analogous calculations give the transmission of the device.

Since our AOS is selective not only to wavelength but also to spatial frequencies, it is necessary to investigate how it filters the different plane waves, which contribute to the spatial spectrum of the Gaussian beam. We considered several cases, starting from normal incidence onto the TMF plane (θ_t = 0). Our investigation showed that the condition θ_t = 0 is absolutely unstable and confirmed the results of [7]. We found that an incidence angle θ_t = 8° represents a reasonable trade-off between the required stability conditions and an unacceptable increase of the spot size impinging on the sample as θ_t approaches 90°. This stability condition can be evaluated by referring to Figs. 7(a), 7(b), where three different R-T curves are plotted versus λ, which correspond to input plane waves having slightly different θ_t values around 8°. The graphics, which refer to the case described in Figs. 4(a), 4(b), show roughly what happens

#93140 - $15.00 USD Received 25 Feb 2008; revised 3 Apr 2008; accepted 3 Apr 2008; published 20 Jun 2008

Table 3. Variations of the extinction ratios η with respect to Tab.1 for changes in amplitude (ΔA), modulus of dielectric constant of gold ($\Delta|\varepsilon_{Au}|$) and thickness of gold layer (Δd) for a 2 NL layers system at λ = 1502.52 nm.Transmission and reflection cases are considered with different pulse durations t_0

Pulse duration t_0 (ps)		$\Delta\eta = \Delta\,(S_{max}/S_{min})$					
		ΔA		$\Delta\|\varepsilon_{Au}\|$		Δd	
		+1 nm	-1 nm	+2%	-2%	+0.2 nm	-0.2 nm
Transmission	5	+0.3	+0.6	+0.1	+0.9	+0.8	+0.5
	10	+0.9	+0.8	0	+1.8	+1.5	+1
	20	-1.8	-0.4	-3.8	-1.3	-1.2	-2.3
Reflection	5	-0.1	+0.2	+0.4	-0.9	+0.3	-0.7
	10	-0.2	+0.2	+1.2	-1.8	-0.8	-1.6
	20	-0.2	+0.3	+1.8	-2.4	-1.4	-2.3

when the two gates are in the OFF state: a variation of θ_t by an amount as small as 0.008°, corresponding to a signal bandwidth of 0.5 nm, leads to a valuable increase of the OFF signal, in particular at the reflectivity gate. To better evaluate this effect we used eq. 6 in the case of three non monochromatic plane input waves, impinging on the structures, illustrated in Figs. 3, 4, 5, 6 at angles 8° and 8° ± γ, where γ is the angular tolerance. Its upper limit is fixed by the need to comply with task #1. Since the curve shifts obtained for the three angles were small, we evaluated the total signal by simply averaging them, instead of performing an exact integration over angle 2γ. However, since we attributed the same weight to the three spatial frequencies, we can infer that our results are generally conservative. Tab. 1 summarizes the results obtained for the two cases of PTS - based AOS corresponding to Figs. 3 and 4. Three lengths of the signal pulses were considered, 5, 10, 20 ps, that is 10 dB bandwidths of 140, 70, 35 GHz respectively. It is noticeable that, in the case of two NL layers, the 20 dB target can be approached even with a 5 ps pulse (140 GHz bandwidth). Table 2 refers to the cases where a purely real and enhanced nonlinearity was considered (Figs. 5, 6). Here one NL layer is sufficient to approach the target figure of 20 dB with 5 ps pulses. In the last case also the switching peak power is reduced to 5.5 kW, comparable with the values found in the case of fibre grating switches [19,20]. In any case, however, the angular tolerance γ is very low. This imposes severe, although technically achievable, constraints to the alignment [21] and to the wavefront curvature.

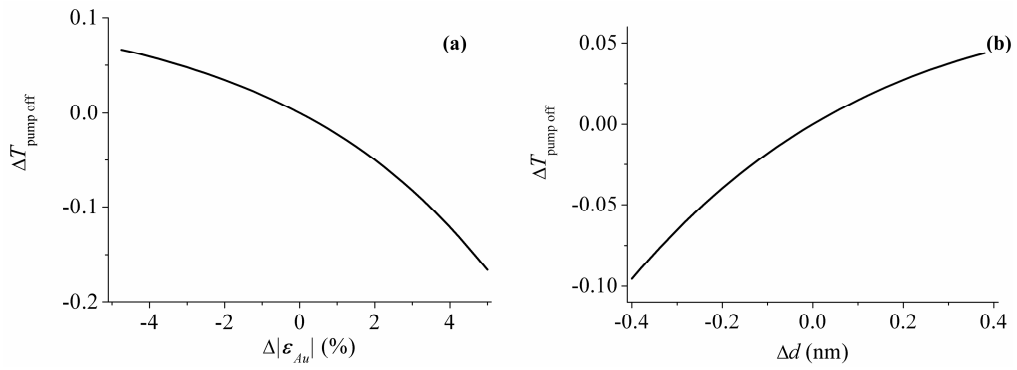

Fig. 9. Transmittivity variations ΔT versus $\Delta|\varepsilon_{Au}|$ **(a)** and Δd **(b)**

#93140 - $15.00 USD Received 25 Feb 2008; revised 3 Apr 2008; accepted 3 Apr 2008; published 20 Jun 2008

2.3 Dimensions of the active volume

We consider a TEM_{00} Gaussian beam with a waist radius w_0 and an incidence angle $\theta_t = 8°$ on the plane *xz* (Fig. 8). A bigger w_0 implies narrower angular spectrum and smaller wavefront curvature in the near field. On the other hand, it also implies higher pump power in order to maintain the correct switching intensity. It is then important to find working conditions, which permit to minimize the wavefront curvature, while maintaining the power-intensity budgets of Tab. 1. For this purpose we start from the phase of the Gaussian input, described by:

$$\Phi(x',y',z') = k\, z' - \mathrm{arctg}\left(\frac{z'}{z_r}\right) + k\frac{\left(x'^2+y'^2\right)}{2\rho(z')} \tag{9}$$

where z_r is the Rayleigh range, and $\rho(z')$ is the curvature radius given by

$$\rho(z') = z'\left[1+\left(\frac{z_r}{z'}\right)^2\right] \tag{10}$$

The propagating wavefronts are exactly planar for $z' = 0$, but the subsequent propagation introduces a distortion. The local wavevectors are no more parallel to the beam axis, as on the beam waist, but they form an angle δ with respect to it, that depends on the position on the wavefront. In the following we consider the worst case, which occurs, moving along *x* axis, at symmetric positions $x = \pm \sec(8°) w_0$. The deflection from beam axis will be referred as δ_x. The wavevector direction can be obtained from the relation

$$\nabla\Phi\,(x',y',z') = k\,\mathbf{s} \tag{11}$$

where **s** is a unit vector normal to the wavefront and δ_x can be expressed at the first order by s_x / s_z , that depends on w_0 and must be equal to the angular tolerance γ of Tab. 1. We increased the input beam waist radius until δ_x matches the tolerances found in Tab. 1. As a result, in the case of a single NL layer, the input beam should have a waist radius of 24 μm, while in the case of two NL layers w_0 can be lowered to 12.5 μm. The dimension of w_0 determines the minimum sections of the pump beam and the illuminated active area. An active volume equal to $\pi \cdot (24\ \mu m)^2$ x 6 μm = 1.086 x 10^{-5} mm^3 and $\pi \cdot (12.5\ \mu m)^2$ x 9 μm = 4.41 x 10^{-6} mm^3 is thus derived for the two cases with complex nonlinearity. In the cases of improved NL response, smaller volumes are allowed with the same intensity budgets. The sub-mm requirement for the dimensions of the device (task #3) is thus theoretically accomplished.

3. A brief survey of AOS fabrication problems

3.1 Fabrication tolerances and characterization of sinusoidally corrugated thin metal films

The expected AOS performances are very sensitive to the values of three parameters: the TMF thickness *d*, the grating amplitude *A* and the metal dielectric constant ε_{Au} . To elucidate this point let us refer to the particular case depicted in Fig. 5. Our numerical simulations considered a deviation from the exact values of *A*, *d* and ε_{Au} given by: $\Delta A = \pm 1$ nm, $\Delta|\varepsilon_{Au}| = \pm 2\%$ and $\Delta d = \pm 0.2$ nm. In practice such tolerances seem to be challenging but not unrealistic. The effects of these errors on the extinction ratio of the two AOS gates are reported in Tab. 3 for the three different pulse lengths. For 5 and 10 ps pulses, the η values of the transmission gate are generally increased, that is the variations of η are positive, with $\Delta\eta$ values in the range 0 - 1.8. On the contrary, for 20 ps pulses $\Delta\eta$ is negative, down to – 3.8 dB but fortunately in this

#93140 - $15.00 USD Received 25 Feb 2008; revised 3 Apr 2008; accepted 3 Apr 2008; published 20 Jun 2008

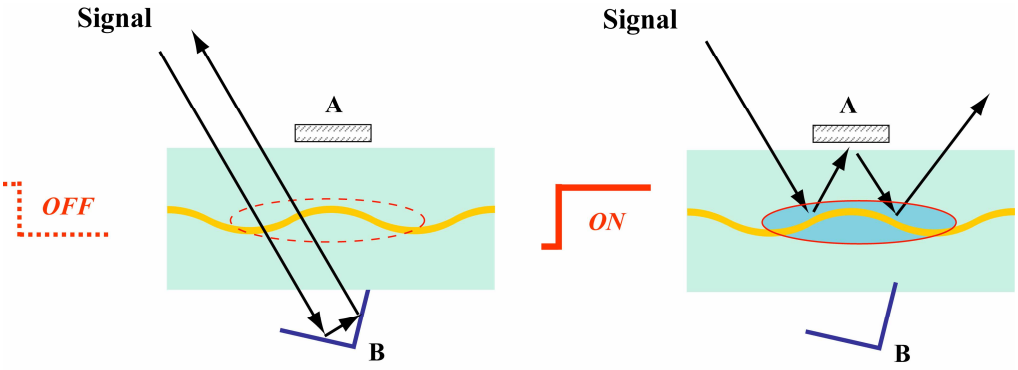

Fig. 10. A possible implementation of the NL AOS . (A = mirrored surface, B = corner cube reflector). The double passage of signal beam into the nonlinear zone ehnances both transmission and reflection device response.

case η can be still > 20 dBs, thanks to the high extinction ratio found in Tab. 1. At the reflection gate the highest decreases of η were found for 20 ps pulses, as far as d and ε_{Au} are concerned, while an error of ± 1 nm in the amplitude A seems to have an almost negligible effect on $\Delta\eta$. In practice it seems that in the device realization d and ε_{Au} smaller than the theoretical values must be avoided, while a small excess can be usually tolerated. In any case, errors in the amplitude A greater than ± 1 nm can be tolerated. Even if the results shown in table 3 are just an example, they look quite encouraging since η usually keeps > 20 dB or, in few cases, very close to 20 dB. In the particular case of the reflection gate and 5 ps pulses η is still > 16.5 dB.

Another set of simulations was performed to check the possibility of exploiting the OFF state transmittivity as an experimental tool to measure A, d, ε_{Au}. Indeed this characterization procedure is not affected by the bandwidth of the Gaussian beam since, according to Ref. [22], a 0.5 nm shift of λ gives rise to a relative variation in $|\varepsilon_{Au}|$ of 0.06% , which is negligible with respect to other effects like spatial fluctuations. The resolution of this method can be easily inferred from Fig. 9 where the sensitivity of T vs $\Delta|\varepsilon_{Au}|$ and Δd is shown. For example, referring to the errors on ε_{Au} and d considered in Tab. 3, ΔT variations are 2.5% and 3.5% respectively and thus they can be easily measured. Moreover, with the same concept, three or more wavelengths can be exploited for a more complete and precise characterization of the device. In conclusion the optical method above outlined results to be a very useful tool to characterize the AOS and to point the fabrication problems out. This method can be combined with the measurements by Atomic Force Microscopy which directly measures the amplitude on the overall device area, since its in-plane scanning range is usually larger than AOS size.

3.2 Grating fabrication and NL films

Material requirements and fabrication tolerances of the proposed AOS are very tight. Therefore, it can be useful to consider briefly the challenging steps to fabricate a laboratory demonstrator of the SPP switch. They are:

- fabrication of the grating corrugations on NL films, followed by metal deposition;
- NL optical response and processability of presently available NL materials and possible development of novel nanostructured composites with improved characteristics;
- reproducibility of the d and ε values of the metal grating. The dispersion of ε_{Au} can depend on the structure of the gold deposition, on the morphology of the substrate and on the modality of the condensation process of the metal on it [23].

The choice of the NL material is also a key problem. AOS operation requires refractive

#93140 - $15.00 USD Received 25 Feb 2008; revised 3 Apr 2008; accepted 3 Apr 2008; published 20 Jun 2008

index variations up to $\Delta n \cong 4.5 \times 10^{-3}$, obtained by Kerr effect. Organic polymers like polydiacetylenes seem to be promising at least to realize demonstrators. Referring to PTS, it exhibits ultrafast sub picosecond response, large nonlinear refractive index ($n_2 = 7 \times 10^{-4}$ cm^2/GW at $\lambda = 1500$ nm) with high saturation values and negligible linear and two-photon absorption. Unfortunately, it exhibits also a non negligible three photon absorption coefficient at 1500 nm [18]. Despite this drawback, the switching peak intensity we have considered compare well with the 12 GW/cm^2 which were well tolerated by a PTS crystal as reported in ref. [14]. Therefore there is much chance that PTS can be actually used in AOS demonstrators to be tested for low repetition rate applications (e.g. 100 MHz - 100 KHz), as for instance label processing in optical packet switching networks**.** Although poorly processable, high optical quality monocrystalline PTS films having the dimensions required by our AOS or even larger can be obtained [18]. Moreover, the surface of such crystalline films can also be properly modulated before metal evaporation. Indeed, gratings were patterned on PTS crystals [18], by employing a standard photoresist mask. The written grating in the mask was then transferred into the film by plasma etching. The damage threshold for gold films has been also widely investigated. For instance, intensities as high as 100 GW/cm^2 were reported at 10 ps and λ=1053 nm [24]. Better performances are expected at around 1500 nm, where gold shows a higher reflectance and a smaller penetration depth. Since the nature of the supported LRSPP forbids the presence of a strong EM field inside the gold film, we can infer weak heating effects and, as a consequence, small ε_{Au} variations .

A reduction of the switching peak power to W or mW relies on stronger nonlinearities (1-2 orders of magnitude) and/or in more complex architectures. Limiting ourselves to organic (or organic/inorganic) materials, such high nonlinearities are actively pursued.

The nonlinear response of polydiacetylenes can be improved by exploiting the enhancing effect that can take place at nanostructured metal/dielectric interfaces [25]. This effect is well known at visible wavelengths in the case of molecules adsorbed on silver or gold spherical nanoparticles and can be observed also in the IR in the case of semicontinuous metal layers at the percolation threshold, or in the case of very rough metal/dielectric interfaces [26]. However, in this second case, the small thickness of the molecular layers interested by the enhancement effect is not sufficient for applications to our AOS devices. In this case, a multilayer approach was proposed to enhance the nonlinearity [27]. A different and hopefully more efficient approach to move the enhancement effect towards telecom wavelengths is that of synthesizing composite materials consisting of properly shaped metal nanostructures embedded in a polymer matrix exhibiting third order nonlinear properties. Some preliminary studies in this sense are in progress, such as the modelling and chemical synthesis of gold nanostars or nanocages [28, 29].

The need of strong nonlinearity could probably be relaxed also by introducing more complex designs of the optical layout. Fig. 10 shows an example of such a modified device. In this two-stage AOS, the reflection or transmission are enhanced by a two-pass path, in which the beam experiences two times the NL effects. A rough extimation for a two-pass configuration shows that a gain of the order of 20 dBs in the switching peak power can be expected. provided that a power threshold in the first switching stage is assured, which should be defined in a dedicated design.

Summarizing, although far from being exhaustive, the quick survey above reported stresses the main problems to be faced in order to implement a demonstrator of the AOS namely:

a) processability of the available materials with the requested NL properties. If possible, development of novel nanostructured materials. A good news is that we need only thin NL films and surfaces as small as 10^{-3} - 10^{-2} mm^2 ;
b) fabrication of the grating corrugations on NL films, followed by deposition of the metal film: grating amplitudes of 20 - 40 nm are requested as well as metal film thicknesses < 20 nm. From our simulations, we got a rough extimation of the fabrication tolerances of

#93140 - $15.00 USD Received 25 Feb 2008; revised 3 Apr 2008; accepted 3 Apr 2008; published 20 Jun 2008

the three parameters d, A and ε_{Au} which should be about 0.2 nm, 1 nm, and 2%, respectively;

c) control of the input angle within 0.001° in the device assembly;

d) upgrading of the above outlined characterization procedure of the corrugated films to achieve the requested precision. In particular the measurement of the incidence angle θ_t must be precise within 0.001°.

4. Conclusion

Here we have proposed an AOSs based on a sinusoidally corrugated gold film, bounded by identical dielectric layers which present strong Kerr effects. Such AOS configuration, requiring no NL waveguide propagation, strongly reduces sizes and losses. In particular, it was found that the volume of the device cores was typically < 10^{-4} - 10^{-5} mm^3, while all the device volume without pigtails could be as small as 10^{-2} mm^3. Concerning losses, the results of our modelling showed that, in the two examined cases of one or two NL layers having the NL characteristics of PTS, the pulse energy at the output gates resulted to be about 70% or 80% of the input respectively, with a pulse length of 5 - 10 ps. Another encouraging result was that about 20 dB extinction ratio per gate can be achieved, even if this requires a peak power of the switching beam as high as 11 kW. Although it is available from fiber amplifiers, this peak power could be reduced to about 5 kW with a reasonable increase (25%) of the material NL and/or at the expense of the switching speed. To this purpose, more complex device configurations can be proposed which make better use of the switching power. The fabrication and characterization of the devices above modelled are expected to present challenging problems Nevertheless, the figures above summarized are within reach (or quite near) of presently available materials and technologies. Therefore, the quick development of nanotechnologies and of novel materials supports our hope that photonic switches based on SPP and NL effects as those above modelled can be actually developed in a near future.

Acknowledgments

The authors wish to thank Dr. Ing. Antonella Bogoni (CNIT,Pisa) for fruitful discussions. Funding from the Italian FIRB “Molecules and organic/inorganic hybrid structures for photonics” (contract n.. RBNE01P4JF) is acknowledged. One of the authors (T.D.R.) wishes to thank for the grant achieved in the frame of FIRB 2004 "Molecular compounds and hybrid nanostructured materials with resonant and non resonant optical properties for photonic devices" (contract no. RBNE033KMA).

#93140 - $15.00 USD Received 25 Feb 2008; revised 3 Apr 2008; accepted 3 Apr 2008; published 20 Jun 2008